H1prelim-02-052, April 2002

High P_T Multi-electron Production in ep collisions at HERA

H1 Collaboration

Abstract

High P_T multi-electron production is measured at HERA using 115 pb^{-1} of positron- and electron-proton collisions collected by the H1 experiment. The data show a good overall agreement with the Standard Model predictions, dominated by photon-photon interactions. Six events are observed with a di-electron mass above 100 GeV, where the Standard Model prediction is low.

1 Introduction

In the frame of the Standard Model (SM) the production of multilepton events is possible in ep collisons mainly through photon-photon collisions, where quasi-real photons from electron and proton interact for producing a pair of leptons $\gamma\gamma \rightarrow \ell^+\ell^-$ [1]. The pair production process is therefore an important tool for investigating photon-photon interactions.

At high transverse momenta or low lepton pair invariant masses, other production mechanisms can contribute [2], involving resolved photons emitted from incident particles or internal conversion. Also rare Standard Model processes like Z production and its leptonic decay are expected. In addition, anomalous production of multi-lepton events at high transverse momenta can be a clear indication for signals beyond the Standard Model.

This analysis presents the first multi-electron production measurement at high transverse momentum at HERA.

2 Standard Model Processes and Monte Carlo simulation

Multi-lepton event production at HERA is simulated by using the GRAPE Monte Carlo generator [3]. GRAPE is based on the symbolic graphs calculation system GRACE and simulates full $2 \rightarrow 4$ matrix element at tree level. The proton dissociation is treated in three phase space regions: elastic,quasielastic and inelastic. GRAPE contains $\gamma\gamma$ graphs with interference effect between the scattered and produced electrons. It also takes into account other production processes: internal conversion (diagrams containing the vertex $\gamma \rightarrow e^+e^-$) and Cabbibo Parisi (photon from proton splitting into e^+e^-, with further interaction of one of those with the beam electron). Initial and final state radiation processes (QED and QCD - parton showers) are simulated.

Main experimental backgrounds are processes producing one true electron, where in addition one or more fake electrons (from photons or hadrons) are selected. This background is mainly reduced by using both calorimetic and tracking capabilities of the H1 experiment, as will be described in the next section. Main contributions to the background are expected from NC-DIS where a fake electron from hadrons or radiated photons is selected together with the (true) scattered electron. The elastic Compton process can also contribute if the high P_T photon is misidentified as electron. The Monte Carlo simulation of NC-DIS processes is based on the DJANGO event generator. Compton processes are simulated by using the WABGEN event generator.

3 Electron Identification

Electron candidates are first identified in the H1 calorimeters (LAr and SPACAL) by using standard shower shape algorithms. The remaining clusters - related to hadronic activity - are combined into hadronic jets. Only electron candidates isolated from other electromagnetic clusters and from hadronic jets are considered ($D_{\eta\phi}^{\mathrm{e}-e',e-jets} > 0.5$). Calorimetric isolation is required in order to further supress fake electrons found in the hadronic final state. In order to insure optimal background rejection and accurate detector control, the electron identification is further refined in different polar angle regions as following:

- **Forward region** $5^\circ < \theta_e < 20^\circ$
  - $E_e > 10$ GeV
  - Calorimetic Isolation
- **Central region** $20^\circ < \theta_e < 150^\circ$ (overlap between LAr calorimeter and central tracker)
  - $E_e > 5$ GeV
  - Calorimetic isolation
  - Good track associated
- **Backward region** $150^\circ < \theta_e < 175^\circ$
  - $E_e > 5$ GeV

4 Event selection

The events are selected if they contain at least two electrons:

- at least a central electron with $P_T > 10$ GeV
- at least a second central electron with $P_T > 5$ GeV

The electron candidates in the event are then classified by decreasing transverse momentum: $\{e_1, e_2, e_3...\}$ with $P_T^{e_1} > P_T^{e_2} > P_T^{e_3}$....

The selected events are classified in event samples as a function of the number of visible electrons in the event as following:

Sample	**Comment**
Visible 2e	Only the two central electrons are visible in the event
Visible 3e	Three electrons are visible in the event
Visible ≥4e	Four or more electrons visible in the event
$\gamma\gamma \to e^+e^-$	Exactly two electrons detected, with associated tracks being of opposite sign and global $E - P_z < 45$ GeV. In this sample, the “scattered” electron is expected to be lost down the beam pipe and the incoming photon bound to be quasi-real ($Q^2 < 1$ GeV). This sample is used to measure the cross section in a well defined phase space with low background.

The results obtained for the HERA I data sample (36.5 pb^{-1} e$^+$p at $\sqrt{s} = 300$ GeV, 13.6 pb^{-1} e$^-$p at $\sqrt{s} = 318$ GeV, 65.1 pb^{-1} e$^+$p at $\sqrt{s} = 318$ GeV, in total 115 pb^{-1}) are shown in table 1. Clear di-electron and tri-electron event samples are selected in the data, in good overall agreement with the expectation. No event with more than three visible electrons is seen in the data (0.1 expected). Global variables related to the event topology are presented in figure 1. Electron transverse momenta and polar angles are presented in the figure 2 and 3. The invariant mass of the two highest P_T electrons in the event and its correlation with respect to the sum of P_T's are shown in the figure 4. The event rates from data compared with the SM expectation for masses above 100 GeV are presented in the table 2. Three di-electron events with masses above 100 GeV are observed for an expectation of 0.25 ± 0.05. In the tri-electron sample, three events with the invariant mass of the two highest P_T electrons above 100 GeV are found for 0.23 ± 0.04 expected. The event displays of the six events at high mass $M_{12} > 100$ GeV are shown in figures 9 to 14. For the tri-electron sample the invariant masses of the electron pairs and also the global three electron mass are shown in the figure 5.

A sample enriched in $\gamma\gamma$ collision processes is used to extract the lepton pair production cross section in the following phase space:

$$\boxed{\begin{array}{c} 20^\circ < \theta_{e_{1,2}} < 150^\circ \\ P_T^{e1} > 10 \text{ GeV}, P_T^{e2} > 5 \text{ GeV} \\ y < 0.82 \\ Q^2 < 1 \text{ GeV}^2 \end{array}}$$

The cross sections measured as function of the hadronic transverse momentum, electron transverse momentum and di-electron invariant mass and presented in the figures 6, 7 and 8.

Control studies related to tracking efficiency, electron mis-identification and photon conversion are presented in the figures 15, 16 and 17.

References

[1] J.A.M.Vermaseren, Nucl.Phys. B229 (1983) 347.

[2] N.Artega-Romero, C.Carimalo, P.Kessler, Zeit.f.Phys C52 (1991) 289.

[3] T.Abe Comp. Phys. Comm. 136 (2001) 126, http://www.awa.tohoku.ac.jp/∼tabe/grape/

H1 Preliminary 115 **pb**$^{-1}$ **Multi-electron Analysis**

Selection	DATA	SM	GRAPE	NC-DIS + Compton
Visible 2e	105	118.2 ± 12.8	93.3 ± 11.5	25.0 ± 5.5
Visible 3e	16	21.6 ± 3.0	21.5 ± 3.0	0.1 ± 0.1
Visible 4e or more	0	0.1 ± 0.0	0.1 ± 0.0	0.0 ± 0.0
$\gamma\gamma \rightarrow e^+e^-$ subsample	41	48.3 ± 6.1	46.4 ± 6.1	1.9 ± 0.9

Table 1: Multi electron event samples together with Standard Model expectation including GRAPE, NC-DIS and Compton predictions. Errors include model uncertainty and experimental systematical errors.

H1 Preliminary 115 **pb**$^{-1}$ **Multi-electron Analysis**

Selection	DATA	SM	GRAPE	NC-DIS + Compton
Visible 2e $M(12) > 100$	3	0.25 ± 0.05	0.21 ± 0.04	0.04 ± 0.03
Visible 3e $M(12) > 100$	3	0.23 ± 0.04	0.23 ± 0.04	0.00 ± 0.00

Table 2: Rates for high di-electron masses $M_{12} > 100$ GeV in the samples with two and three visible electrons.

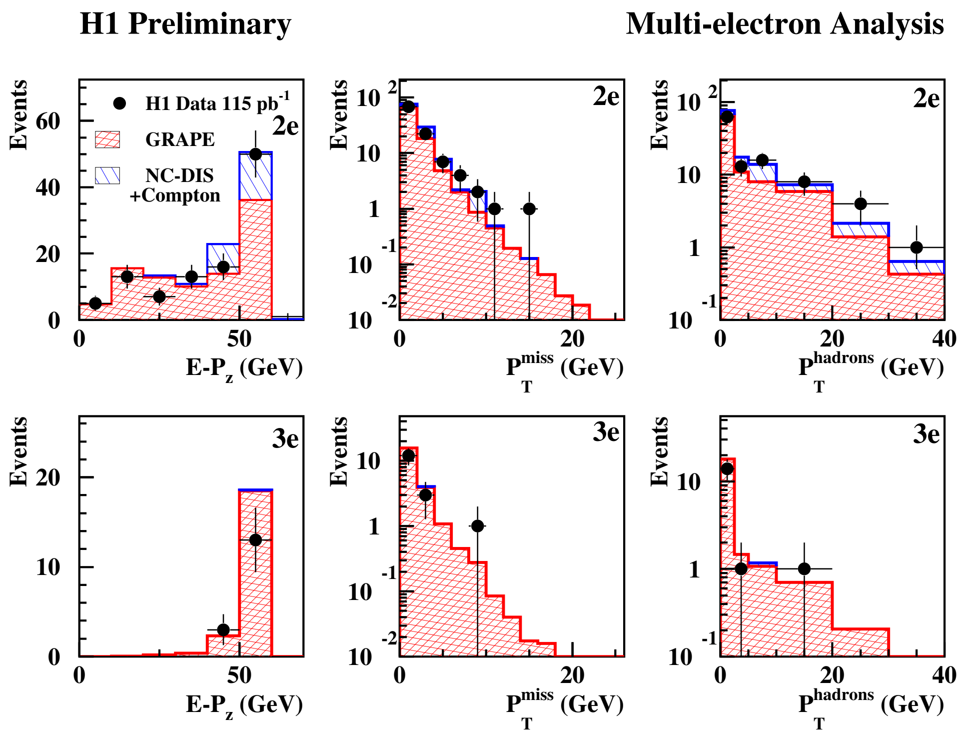

Figure 1: Gloabal variables ($E - P_z$, P_T^{miss} and $P_T^{hadrons}$) for the sample contaning two visible electrons (upper figures) and the sample with three visible electrons (lower figures).

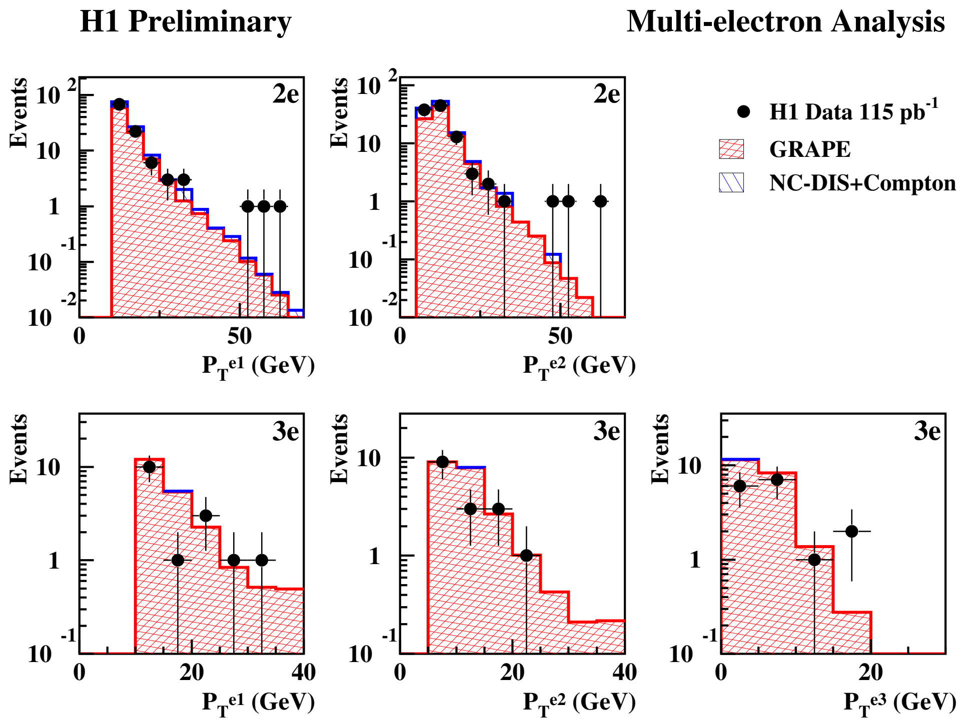

Figure 2: Transverse momenta of the observed electrons in the di-electron sample (upper figures) and tri-electron sample (lower figures).

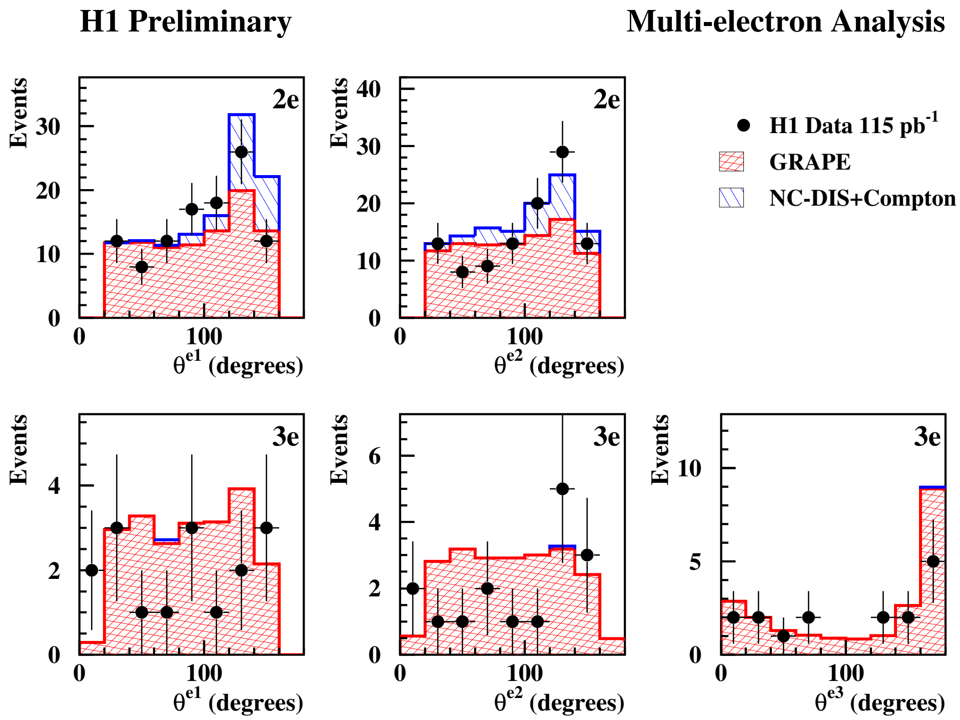

Figure 3: Polar angle (θ) distribution of the observed electrons in the di-electron sample (upper figures) and tri-electron sample (lower figures).

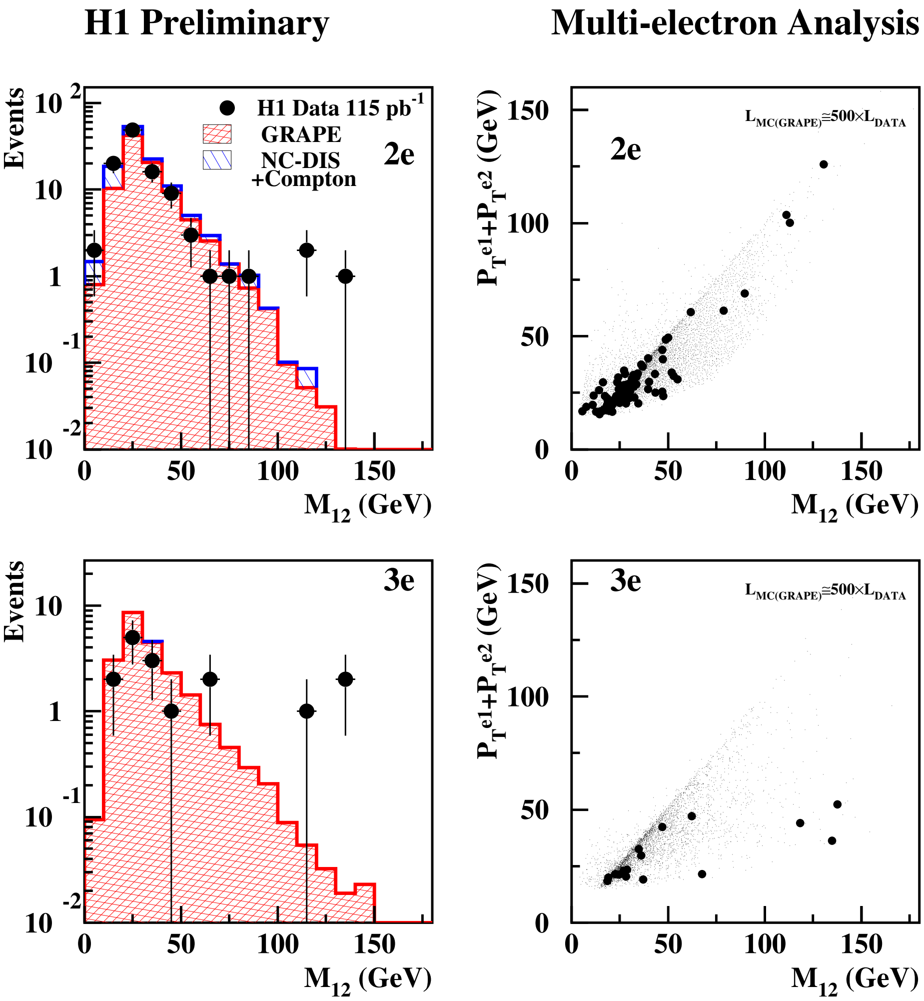

Figure 4: Distribution of invariant mass of the two highest P_T electrons M_{12} (left) and the scatter plot representing the sum of P_T's of the two highest P_T electrons as a function of M_{12} (right). The sample with two visible electrons is shown in the upper figures while the sample with three visible electrons is presented in the lower figures.

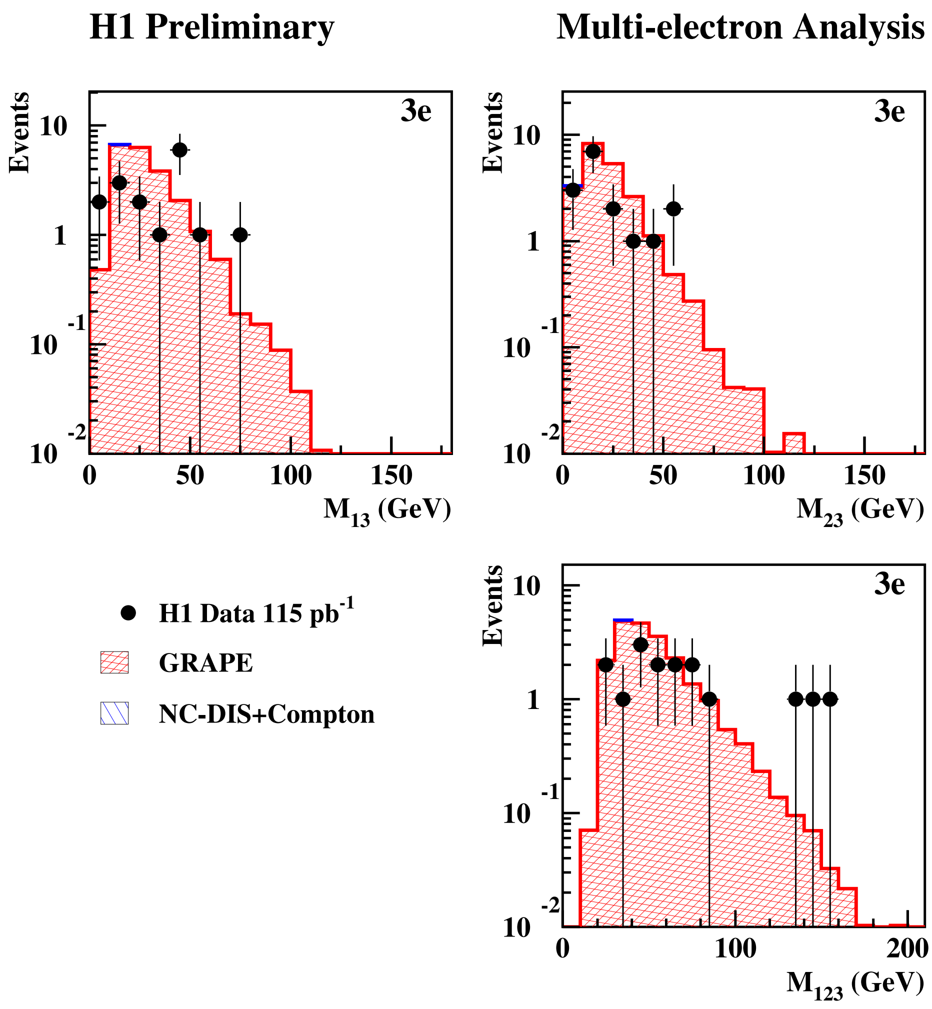

Figure 5: Sample of events with three visible electrons: invariant masses of electron pairs 1-3 and 2-3 (upper figures) and total invariant mass of the three electrons M_{123} (lower figure).

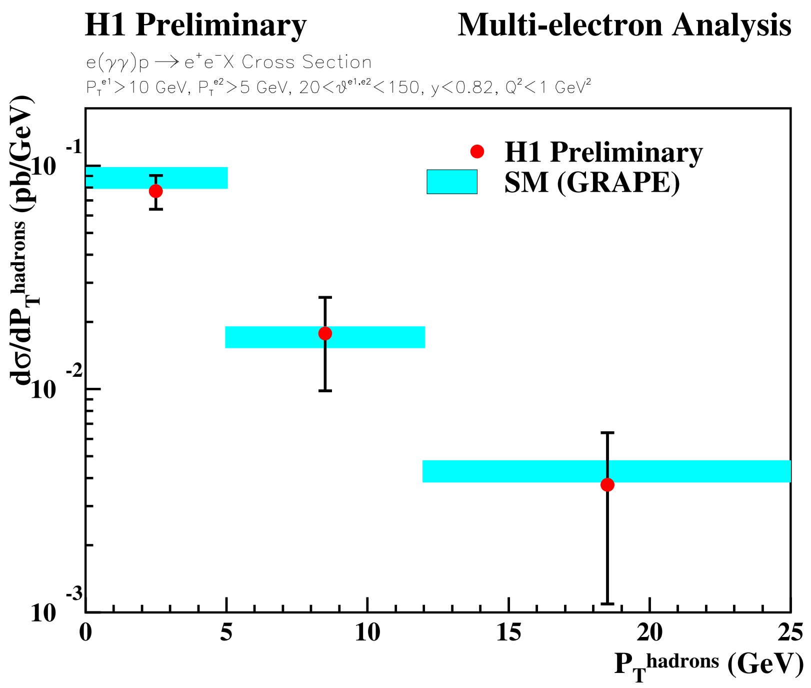

Figure 6: Cross section measurement as a function of the hadronic transverse momentum in the $\gamma\gamma \to e^+e^-$ sample. The phase space of the measurement is defined on top of the figure.

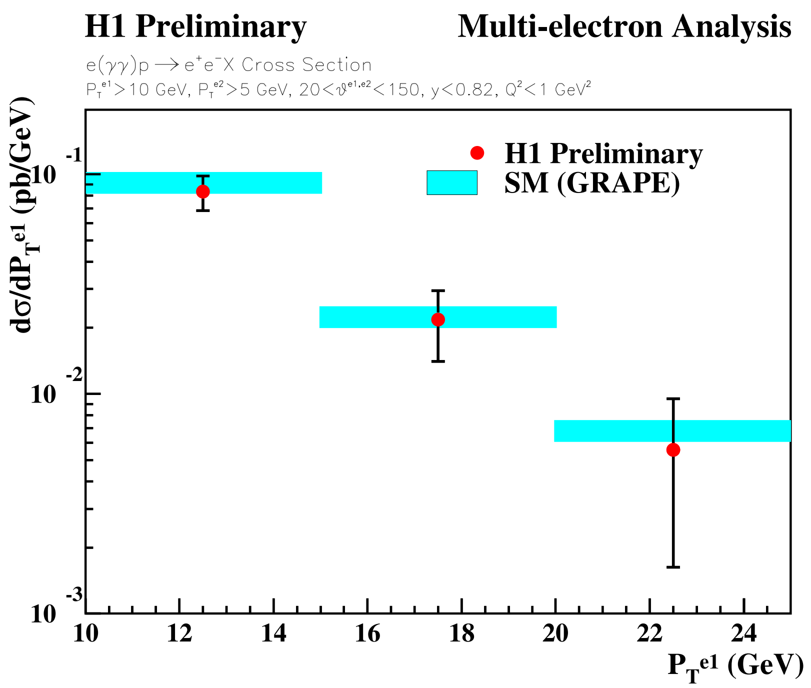

Figure 7: Cross section measurement as a function of the highest electron transverse momentum in the $\gamma\gamma \to e^+e^-$ sample. The phase space of the measurement is defined on top of the figure.

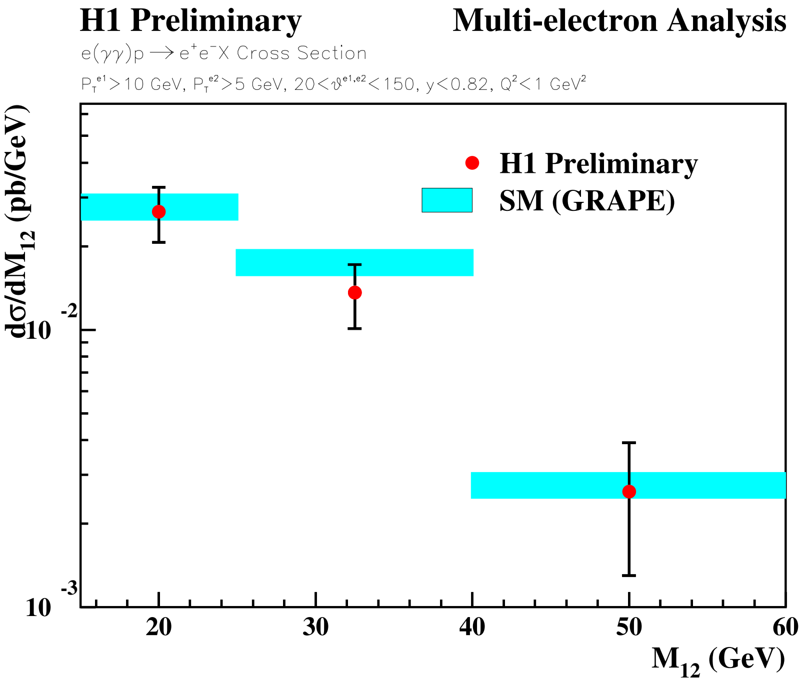

Figure 8: Cross section measurement as a function of electrons invariant mass in the $\gamma\gamma \to e^+e^-$ sample. The phase space of the measurement is defined on top of the figure.

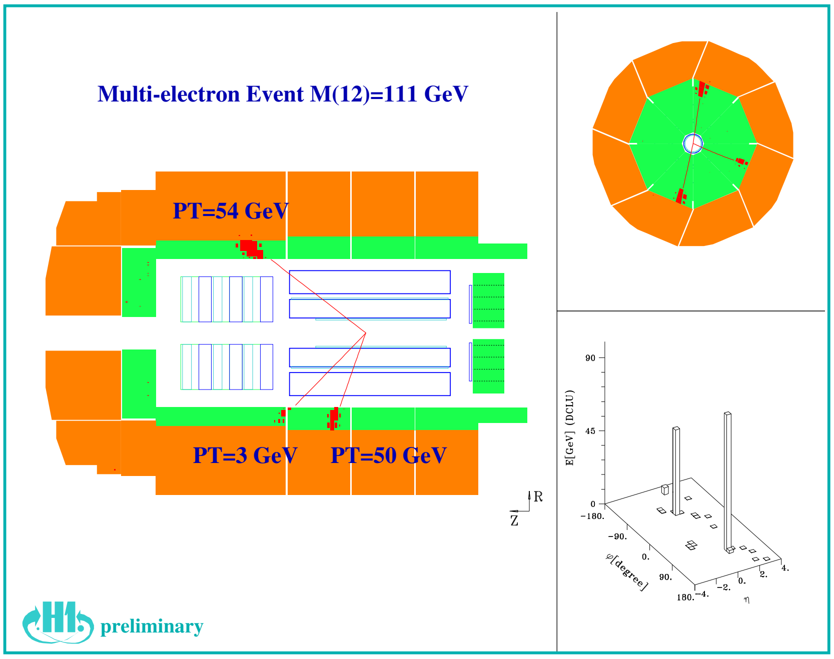

Figure 9: Event Display (Run 83507 Event 16817). The event is selected in the di-electron sample. The lowest P_T electromagnetic cluster does not satisfy the energy threshold requirement ($E > 5$ GeV).

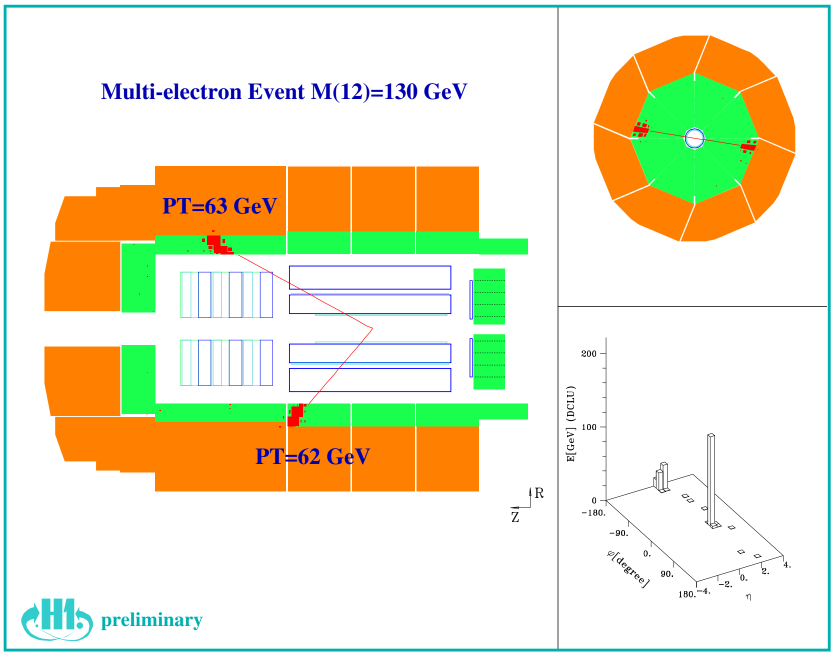

Figure 10: Event Display (Run 89256 Event 224212)

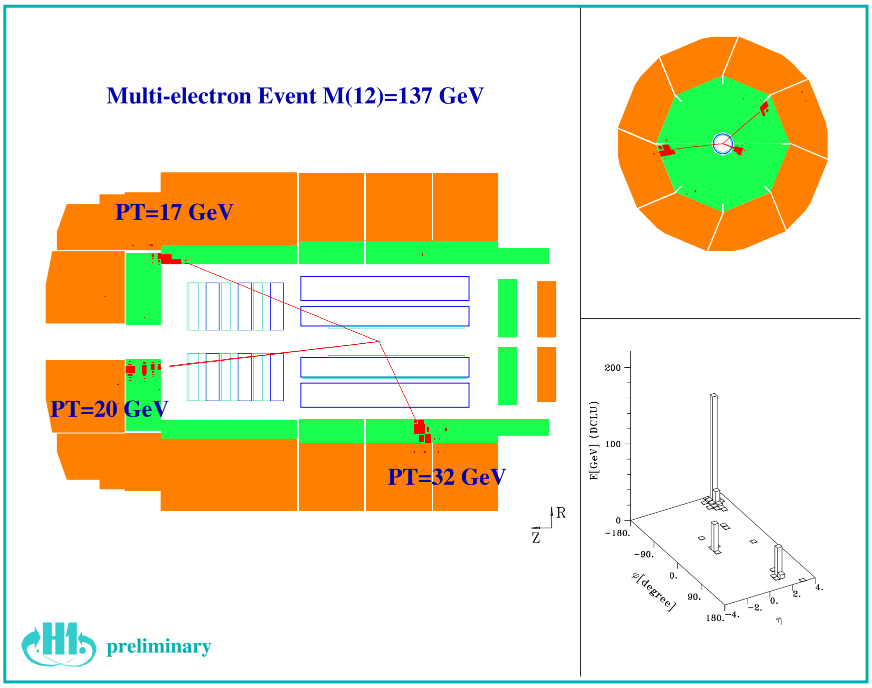

Figure 11: Event Display (Run 168058 Event 42123)

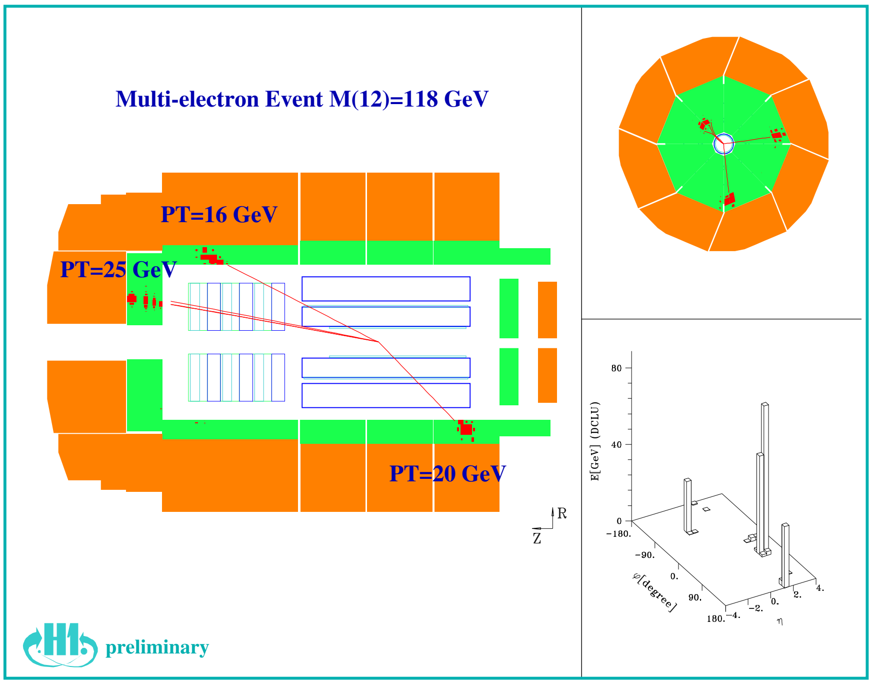

Figure 12: Event Display (Run 192864 Event 123614)

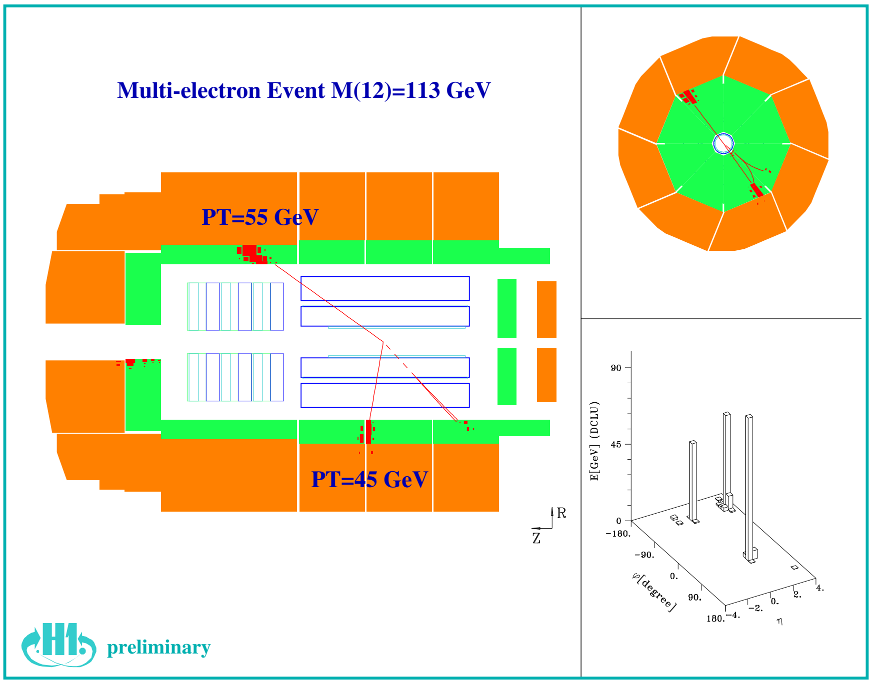

Figure 13: Event Display (Run 254959 Event 17892)

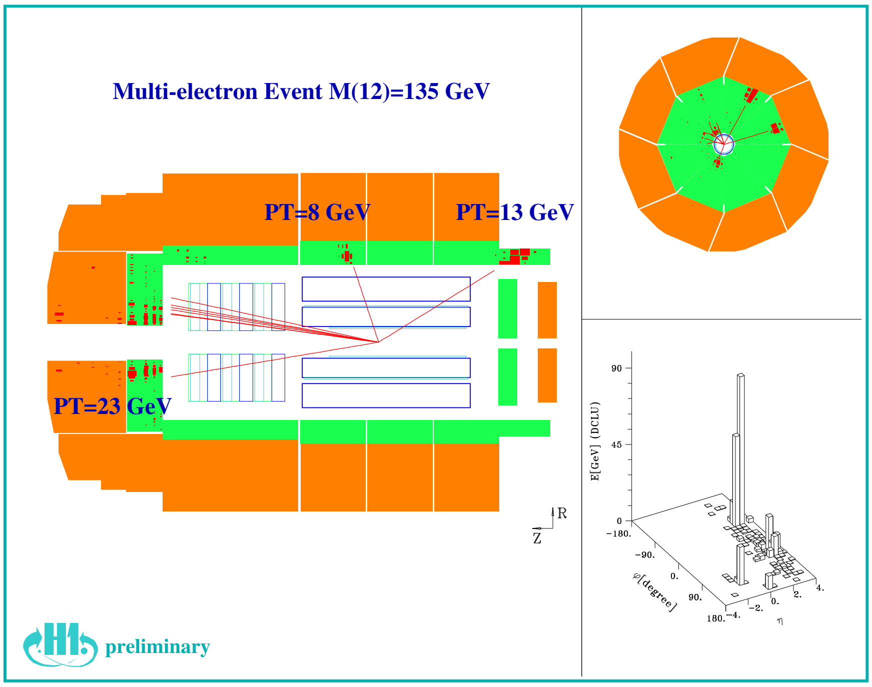

Figure 14: Event Display (Run 267312 Event 203075)

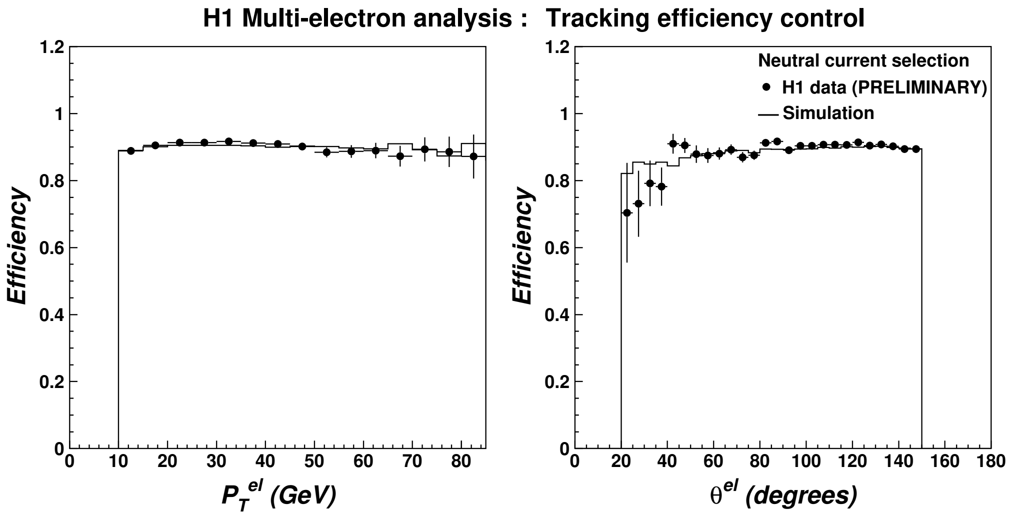

Figure 15: Track association efficiency as function of electron transverse momentum (left figure) and electron polar angle (right figure). The efficiency is calculated by using a sample of neutral current events selected with calorimetric identification algorithms. The systematical uncertainty associated with the tracking is 15% at low polar angle and 3% in the central region.

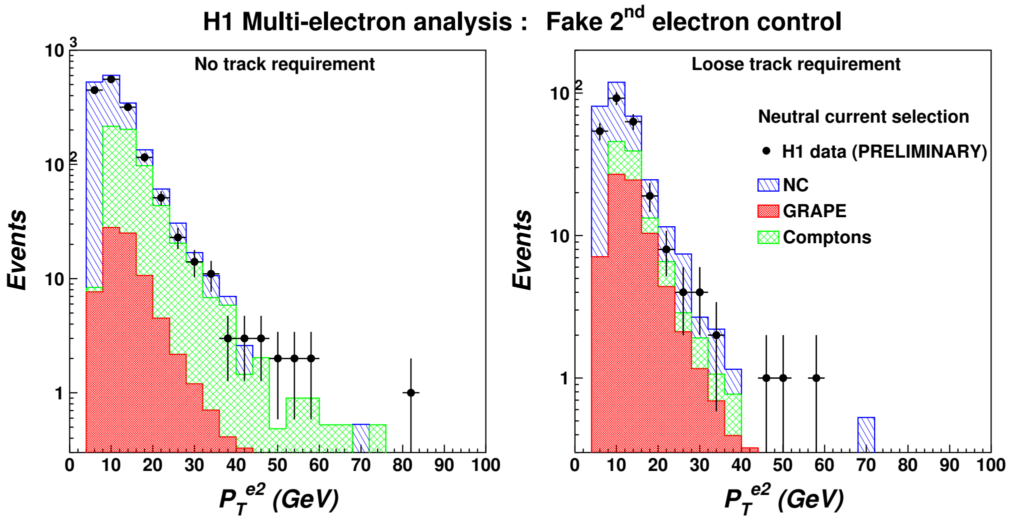

Figure 16: "Second" electron production in a sample selected with a good high P_T electron. The transverse momentum of the second electromagnetic cluster is shown with no tracking requirement (left) and with a loose tracking requirement (right) correspoding to a good track association only (no R_{start}, no track-cluster match conditions). Data is compared with Monte Carlo prediction including GRAPE, NC-DIS and Compton processes. Compton process yields events with two electromagnetic clusters with high transverse momenta (left figure). The track associaton requirement drastically reduce this contribution (right figure). Good agreement between data and Monte Carlo simulation is found in this control sample.

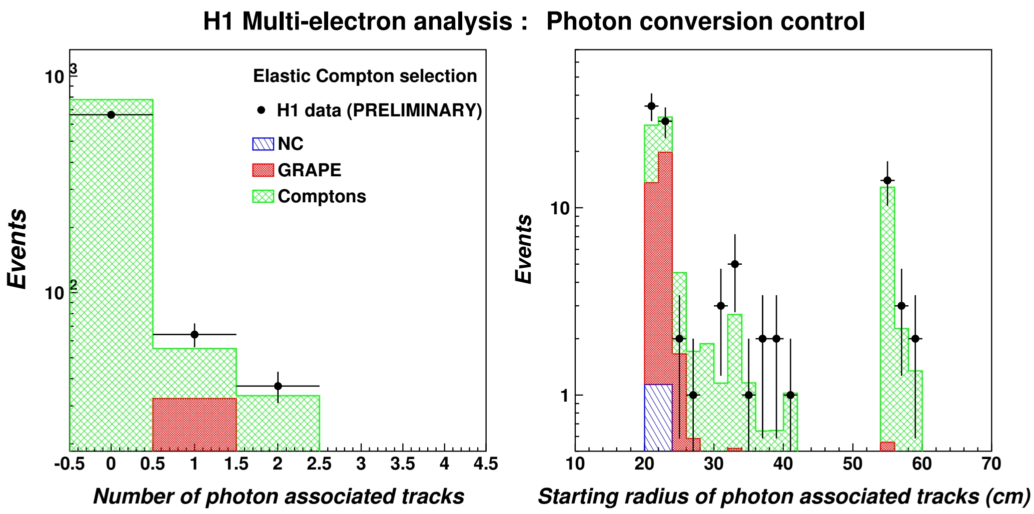

Figure 17: Photon conversion study performed by using a sample with two electromagnetic clusters and low hadronic activity, dominated by elastic Compton process with an electron and a photon in the final state. The number of tracks associated to the photon is shown in the left figure. For the candidates with an associated track, the radius of the first point measured in the central tracking chambers (R_{start}) is shown in the right figure.